Int. J. Solids Structures, 1972, Vol. 8, pp. 297 to 314. Pergamon Press. Printed in Great Britain

THE EFFECT OF SHEAR ON YIELDING OF STRUCTURAL MEMBERS

FERNAND ELLYIN† and ROBERT DELOIN‡

Faculté des sciences appliquées, Université de Sherbrooke,
Sherbrooke, Québec, Canada

Abstract—Interaction surfaces are obtained for structural elements subject to combining axial, shear force, and bending moment. The structural material is rigid-perfectly-plastic, obeying Tresca or von Mises yield criterion. A two hinged circular arch is chosen to demonstrate the application of the preceding theory. The effect of the inclusion of shear force is the lowering of the collapse load. Limits, in which the influence of the shear force on the yielding of arches is considerable, are indicated.

NOTATION

A	cross-sectional area
$2b$	width of flange
d	mean thickness of flange
F	resultant reaction force of arch
F_h, F_v	horizontal and vertical reactions of arch
$2h$	depth of cross-section
M	resultant moment
m	non-dimensional resultant moment
M_0	maximum plastic moment
m_ϕ	non-dimensional resultant moment in arch obtained through division by M_0
N	resultant axial force
n	non-dimensional resultant axial force
N_0	maximum plastic axial force
n_ϕ	non-dimensional resultant axial force in arch obtained through division by N_0
$2P$	force applied in the center of arch
p, q	Euler's multipliers
R	radius of circular arch
t	depth to diameter ratio
$\mathbf{u}$	horizontal velocity at hinge A
V	resultant shear force
v	non-dimensional shear force
v_ϕ	non-dimensional resultant shear force obtained through division by V_0
$\mathbf{v}$	vertical velocity at hinge A
V_0	maximum plastic shear force
W_{ext}	external energy rate
W_{int}	internal energy rate
$2w$	web thickness
x, y, z	rectangular cartesian coordinate system
α	a coefficient in yield criterion
Γ	shearing-rate in general
γ	non-dimensional shearing-rate

† Associate Professor and Head, Structures and Solid Mechanics Section.
‡ Research Engineer.

γ_{xy} shearing-rate in yz plane
Δ shortening-rate in arch
$\Delta\eta$ rate of rotation due to shear in arch
δ non-dimensional geometric coefficient
ε_x normal strain-rate
η rate of rotation due to pure bending in hinge A
θ total rotation rate in arch
$\mathbf{K}$ rate of curvature
Λ shortening-rate in general
λ non-dimensional shortening rate in arch
μ arbitrary positive scalar
ν non-dimensional geometric coefficient
ξ rate of rotation in arch
ρ^- non-dimensional lower bound to limit load
ρ^+ non-dimensional upper bound to limit load
ρ^* non-dimensional limit load without shear influence
σ_x normal stress
σ_0 tensile yield stress of material
τ_{xy} shear stress
ϕ_0 semi-angle of circular arch
ϕ coordinate of arch
χ angle between the resultant reaction force and the tangent to the arch at its support, also, angle of position of hinge B from support
ψ rate of rotation due to pure bending in hinge B
ω non-dimensional geometric coefficient

1. INTRODUCTION

IN THE limit analysis, the effect of shear force in the yielding of structures has been generally neglected. Although this assumption may be justified for "thin walled" structures, its extension to "thicker" ones will induce inaccuracy of an unknown magnitude. The difficulties which one may encounter by including the shear force in yielding of beams has been pointed out by Drucker [1]. He showed that for a given cross-section, a unique interaction curve between the shear force and bending moment does not exist. The geometry and loading of the entire beam enter into the analysis, thus the interaction curve is not just a local matter. Drucker arrived at this conclusion by considering plane-stress fields within the beam, and by employing the upper and lower bound theorems of limit analysis. Using Prager's [2] generalized stress concept, Hodge [3] has derived unique interaction curves for plastic beams subject to combined shear and bending.

In the first part of this paper, interaction surfaces are obtained for structural elements subject to combined shear, normal force, and bending moment. The statically admissible stress field approach, and that of kinematically admissible strain-rate fields, both yield the same interaction surface. The interaction surface obtained herein is, therefore, an exact one. A number of interaction diagrams of previous works are then derived as particular projections of this surface.

A two hinged circular arch is considered in order to apply the present theory. Here too, an exact solution is obtained and the variation of the collapse load with the geometric parameters is discussed. Finally, the collapse load of the arch is calculated without considering the contribution of the shear force on yielding. The predictions of the present theory are compared in the last section of the paper. As expected, the inclusion of the shear force results in lowering the collapse load. The results presented here are believed to be of practical interest in the design of structures where the shear effect is not negligible.

2. INTERACTION SURFACE

2.1 *Statically admissible stress field approach*

For a bending moment M, an axial force N and a shear force V, acting on the plane yz, an appropriate distribution of the stress components σ_x and τ_{xy} will suffice description, Fig. 1. These stress components, for a perfectly plastic material, must also satisfy a yield criterion,

$$\sigma_x^2 + \alpha^2 \tau_{xy}^2 \leq \sigma_0^2 \tag{1}$$

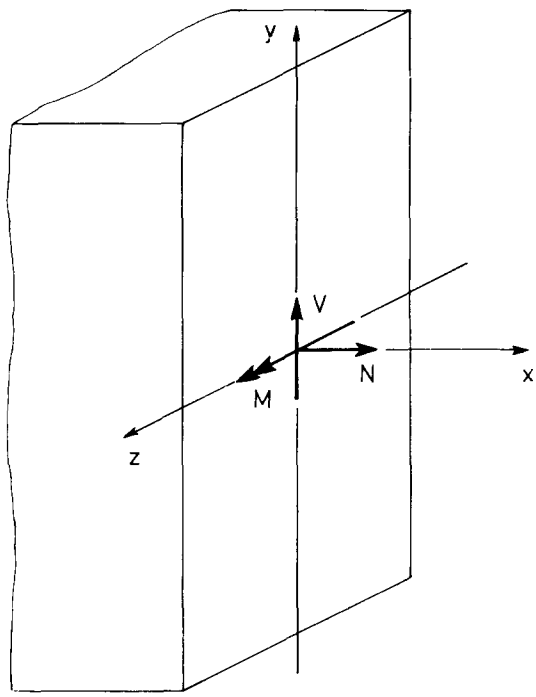

FIG. 1. A structural element subject to bending moment, axial force and shear force.

where σ_0 is the tensile yield stress and α is a coefficient which depends on the chosen yield criterion. For the Tresca yield criterion $\alpha = 2$, whereas for that of von Mises $\alpha = \sqrt{3}$.

In a fully plastic section A, the resultant moment, shear and axial force will then be given by:

$$\begin{aligned} M &= \int_A \sigma_x y \, \mathrm{d}A \\ V &= \int_A \tau_{xy} \, \mathrm{d}A = \frac{1}{\alpha} \int_A (\sigma_0^2 - \sigma_x^2)^{\frac{1}{2}} \, \mathrm{d}A \\ N &= \int_A \sigma_x \, \mathrm{d}A. \end{aligned} \tag{2}$$

The problem of finding the interaction surface may be stated as: given values of M and N, find a function σ_x, so as to maximize V. Assuming that σ_x is not a function of z, the problem thus posed becomes a simple problem in variational calculus. Since the integrands in equations (2) contain only σ_x and none of its derivatives, the Euler equation will therefore become finite instead of differential. Furthermore, because of symmetry, one needs only to consider the first trihedral of the M,N,V-space. With the Euler multipliers denoted by p and q, the Euler equation becomes:

$$\frac{\partial}{\partial\sigma_x}\left[\frac{1}{\alpha}(\sigma_0^2-\sigma_x^2)^{\frac{1}{2}}\right]+p\frac{\partial}{\partial\sigma_x}(\sigma_x)+q\frac{\partial}{\partial\sigma_x}(\sigma_x y)=0 \tag{3}$$

from which,

$$\sigma_x=\alpha\sigma_0(p+qy)[1+\alpha^2(p+qy)^2]^{-\frac{1}{2}}. \tag{4}$$

The resultant stresses are then obtained from substituting equation (4) into (2):

$$\begin{aligned} M &= \alpha\sigma_0\int_A (p+qy)[1+\alpha^2(p+qy)^2]^{-\frac{1}{2}}y\,\mathrm{d}A \\ N &= \alpha\sigma_0\int_A (p+qy)[1+\alpha^2(p+qy)^2]^{-\frac{1}{2}}\,\mathrm{d}A \\ V &= \frac{\sigma_0}{\alpha}\int_A [1+\alpha^2(p+qy)^2]^{-\frac{1}{2}}\,\mathrm{d}A. \end{aligned} \tag{5}$$

2.2 *Kinematically admissible strain-rate approach*

If the deformation is assumed to be a combination of pure bending, uniform shear and compression (or tension), then one has:

$$\begin{aligned} \varepsilon_x &= \mathbf{K}y+\Lambda \\ \gamma_{xy} &= \Gamma \end{aligned} \tag{6}$$

where $\mathbf{K}$, Λ and Γ are constant for a given plastic section. Substitution of (6) in the expression for the rate of dissipation of energy for a section, will then show that $\mathbf{K}$, Λ and Γ are the appropriate strain-rates to be associated with the generalized stresses M, N and V, respectively. Proceeding in a manner similar to that of Ref. [3], one will arrive at a set of equations identical to those of (5). Therefore, the interaction surface represented by the integrals (5) in terms of variables p and q is an exact one, of course, within the assumptions inherent in the limit analysis. It may be noted that by setting $\alpha = 2$ and $N = 0$ in equations (5), one recovers the integral equations for the bending moment and shear force obtained by Hodge [3]. It should be noted that the equivalency of static and kinematic approaches is achieved by using Drucker's postulate of a "stable material" [4]. This assumption implies convexity of the interaction surface. Recently Heyman [5] has pointed out that for a cantilever, interaction diagram between M and V is not a proper yield surface and thus the convexity does not hold. The arguments advanced in [5] however, do not seem applicable for the example treated hereinafter.

2.3 *Parametric equations of the interaction surface*

Calculations will be first performed for an *I*-section as shown in Fig. 2. The maximum plastic moment, axial and shear force that a given section may support are:

$$M_0 = 2\sigma_0 bh^2 CM$$
$$N_0 = 4\sigma_0 bhC \tag{7}$$
$$V_0 = \frac{4}{\alpha}\sigma_0 bhC$$

where,

$$CM = (2-\delta)\delta + (1-\delta)\omega$$
$$C = \delta + (1-\delta)\omega$$

with $\delta = d/h$ and $\omega = w/b$, representing dimensionless geometric parameters. Note that specific variation of the non-dimensional parameters δ and ω, will generate the following sections:

rectangle, when $\omega = 1, \quad \delta = 0,$

ideal *I*-section (sandwich), when $\omega = 0, \quad \delta = \delta_0,$

I-section, when $\omega = \omega_0, \quad \delta = \delta_0.$

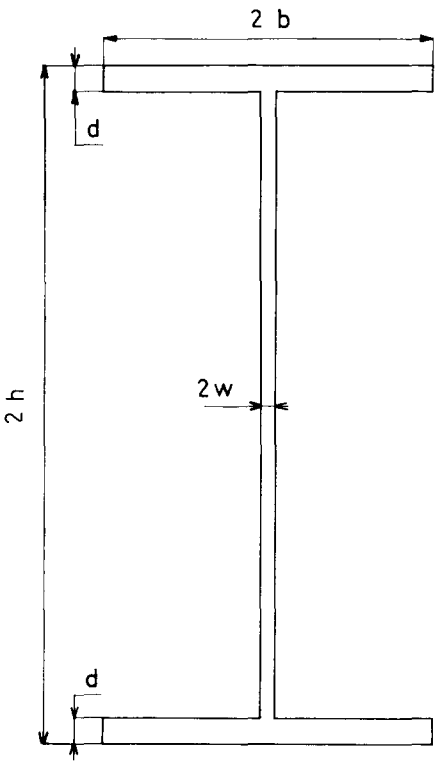

FIG. 2. An *I*-cross-section.

A third non-dimensional parameter, say $v = \omega/\delta = wh/bd$, will then complete the description of the geometry of the sections.

In order to simplify the results of the integrals (5), let:

$$\begin{aligned} r &= \alpha p, \\ s &= \alpha q h \end{aligned} \tag{8}$$

and

$$\begin{aligned} SS &= r+s \\ SD &= r+s(1-\delta) \\ DS &= r-s \\ DD &= r-s(1-\delta). \end{aligned}$$

It may be easily verified that for the I-section of Fig. 2, and the parameters defined by relations (7) and (8), the evaluated integrals (5) have the following form:

$$\begin{aligned} m(r,s) = \frac{M}{M_0} &= \frac{1-\omega}{2s^2CM}[DD(1+SD^2)^{\frac{1}{2}} + \sinh^{-1}(SD) - SD(1+DD^2)^{\frac{1}{2}} - \sinh^{-1}(DD)] \\ &\quad + \frac{1}{2s^2CM}[SS(1+DS^2)^{\frac{1}{2}} + \sinh^{-1}(DS) - DS(1+SS^2)^{\frac{1}{2}} - \sinh^{-1}(SS)] \\ n(r,s) = \frac{N}{N_0} &= \frac{1-\omega}{2sC}[\sinh^{-1}(DD) - \sinh^{-1}(SD)] + \frac{1}{2sC}[\sinh^{-1}(SS) - \sinh^{-1}(DS)] \\ v(r,s) = \frac{V}{V_0} &= \frac{1-\omega}{2sC}[(1+DD^2)^{\frac{1}{2}} - (1-SD^2)^{\frac{1}{2}}] + \frac{1}{2sC}[(1+SS^2)^{\frac{1}{2}} - (1+DS^2)^{\frac{1}{2}}]. \end{aligned} \tag{9}$$

Part of the interaction surface constructed from (9) for a rectangular section and Tresca material is shown in Fig. 3. The remaining parts may be obtained by considering symmetry with respect to the three planes. The interaction curves for various profiles, obtained by the intersection of the plane $V = 0$, are shown in Fig. 4. For a rectangular cross-section, this interaction curve was first investigated by Onat and Prager [6], and for other sections, one recovers the classical results [7]. Figure 5 indicates the interaction diagram obtained through the intersection with the plane $N = 0$. The results of this particular case correspond to the problem treated by Hodge [3]. There is a very small difference between curves presented here and those of Ref. [3]. This is due to neglect of higher than the first-order terms in ω and δ, in Hodge's work. The interaction curve resulting from the intersection with the plane $M = 0$ is given by equation

$$n^2 + v^2 = 1 \tag{10}$$

and is independent of the shape of the section.† Note that most of the rolled wide-flange sections fall within the limits shown in Figs. 4, 5, and the extreme curves for rectangular and sandwich sections may be regarded as upper and lower limits, respectively.

† Neglecting M in equations (2) and proceeding with the variational problem: given N, what is the function σ_x which maximizes V? one will find the equation of a circle, independent of the cross-section.

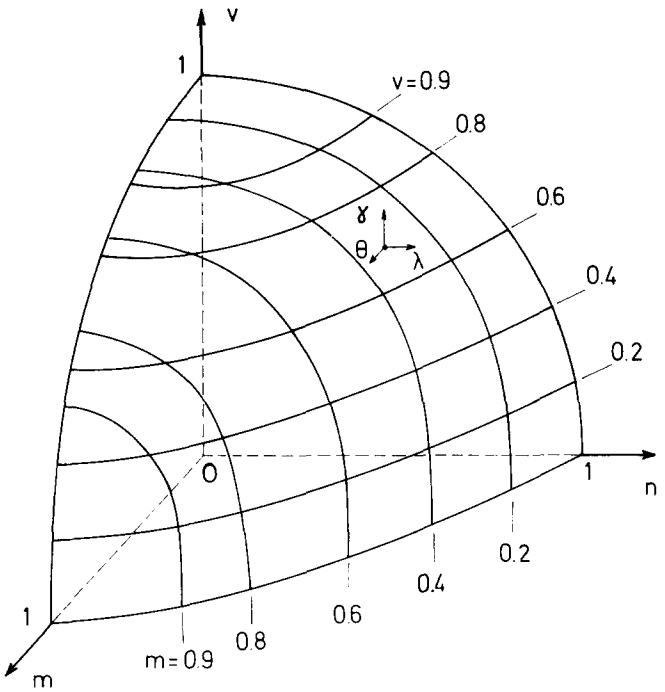

FIG. 3. Interaction surface for a rectangular cross-section.

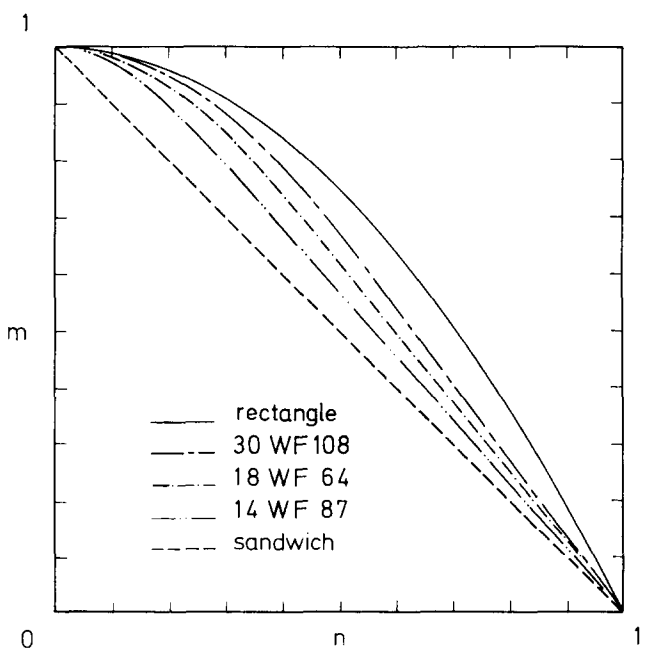

FIG. 4. Intersection profile with plane $V = 0$.

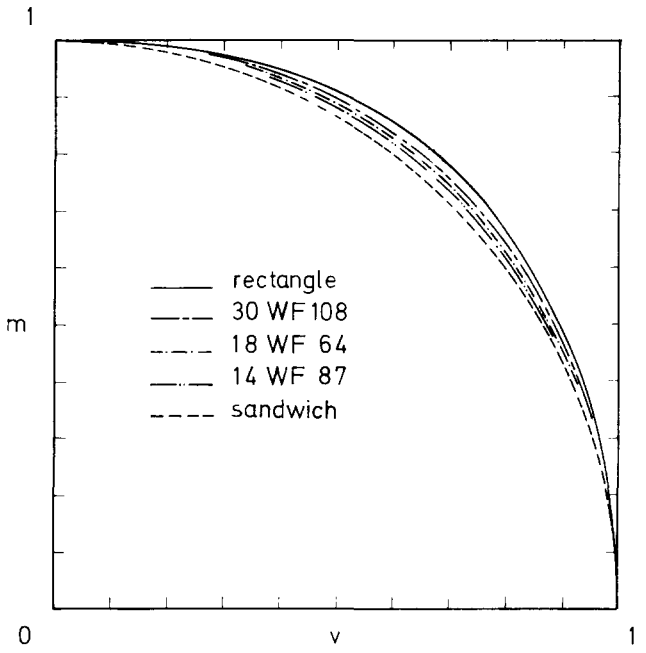

FIG. 5. Intersection profile with plane $N = 0$.

Various projections of the interaction surface with the plane v = const. are shown in Fig. 6. It may be noted that as long as $V \leq 0{\cdot}2V_0$, the effect of shear force on the interaction diagram M–N, is negligible. When $V \geq 0{\cdot}6V_0$, the effect of the shear force becomes quite pronounced. The latter case, for example, may arise when the web of an I-section is fully yielding in shear.

3. APPLICATION

A simply supported circular arch is chosen to illustrate the application of the interaction surface derived in the previous sections.

Let the arch with radius R, subtending an angle $2\phi_0$, be of rectangular section (Fig. 7). A concentrated force of $2P$ is applied at its center. Due to symmetry, the vertical reaction at each support is $F_v = P$, and the horizontal reaction F_h is the only unknown redundant. However, for the sake of convenience, the angle χ between the resultant reaction force F, and the tangent to the arch at its support, will be taken as the unknown redundant. The following nondimensional parameters will be adopted in the analysis to follow:

$$\rho = \frac{PR}{M_0}, \qquad CA = \frac{CM}{C}\frac{h}{R} \tag{11}$$

where h is the half thickness of the arch. In this manner ρ becomes a dimensionless load parameter and CA a dimensionless geometric parameter. In the case of a rectangular section, CA becomes the thickness to diameter ratio.

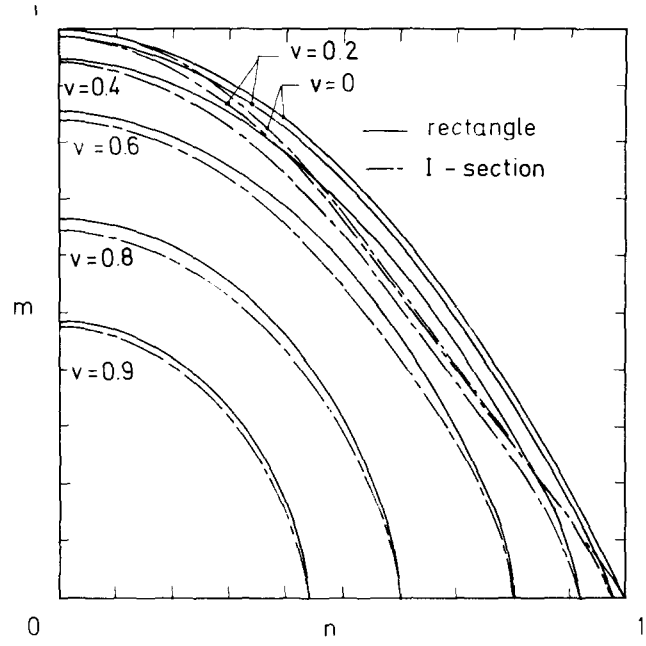

FIG. 6. Intersection profiles with planes V = const.

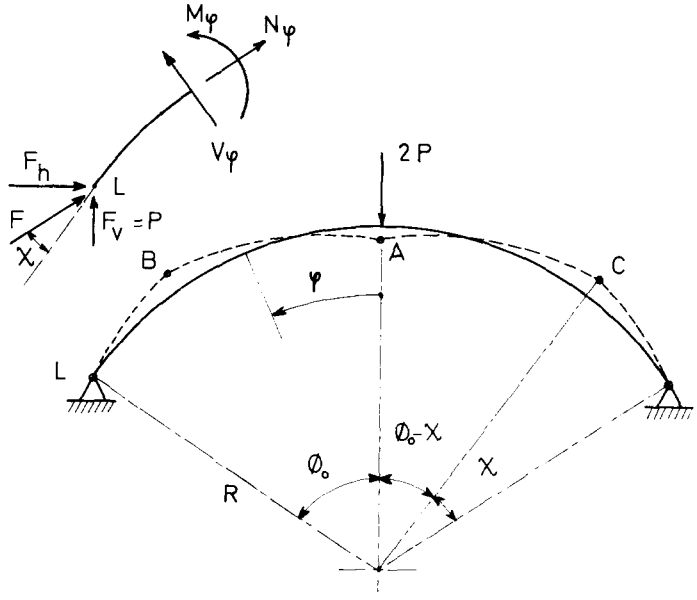

FIG. 7. A simply supported circular arch subject to concentrated load at its center, with appropriate notations.

Equilibrium of a free body section (Fig. 7) of the arch yields:

$$m_\phi = \rho \frac{\cos\chi - \cos(\phi - \phi_0 + \chi)}{\sin(\phi_0 - \chi)}$$

$$n_\phi = -\tfrac{1}{2}\rho CA \frac{\cos(\phi - \phi_0 + \chi)}{\sin(\phi_0 - \chi)} \tag{12}$$

$$v_\phi = -\frac{\alpha}{2}\rho CA \frac{\sin(\phi - \phi_0 + \chi)}{\sin(\phi_0 - \chi)}.$$

Note that the coordinate angle ϕ is measured from the center of the arch. The collapse mechanism is shown by the dashed line in Fig. 7. Plastic hinges form at points subtended by angles $\phi = 0$ and $\phi = \phi_0 - \chi$. Note that hinges B and C may be chosen such that they correspond to the position of the maximum bending moment, thus $v(B) = v(C) = 0$.

3.1 *Lower bound analysis*

At hinge B, the relation between bending moment and axial force is given by (see Fig. 4 or Ref. [6]):

$$-m_B = 1 - n_B^2. \tag{13}$$

Substituting the appropriate values from (12) in the above relationship yields,

$$\rho^- = \frac{2}{CA^2}\sin(\phi_0 - \chi)\{[(1-\cos\chi)^2 + CA^2]^{\frac{1}{2}} - (1-\cos\chi)\}. \tag{14}$$

The variable χ has to be determined so that a lower bound on the collapse load can be calculated. This is achieved by observing that the stress vector at point A is also on the yield surface. The stress values at this point are obtained by substituting $\phi = 0$ in equations (12). The requirement that the stress point be on the yield surface is obtained through equating equations (9) and (12) for point A. The result is a system of three non-linear equations:

$$\begin{aligned} m_A &= m(r, s) \\ n_A &= n(r, s) \\ v_A &= v(r, s) \end{aligned} \tag{15}$$

which has to be resolved. Note that the left-hand side of (15) is a function of χ only. The χ obtained from (15) is then substituted in equation (14) to obtain a lower bound ρ^-, to the collapse load.

3.2 *Upper bound analysis*

The collapse mechanism of Fig. 7 requires formation of three hinges. In each of these hinges, there will generally be three deformation modes, namely, rotation due to bending moment, shortening due to axial force and shear deformation due to shear force. Figure 8 shows these deformation patterns for the central hinge A.

Let η; ψ, denote the angles of rotation due to pure bending and Δ_A; Δ_B, shortening caused by the axial force at hinge A and B, respectively. Then the deformed arch at the

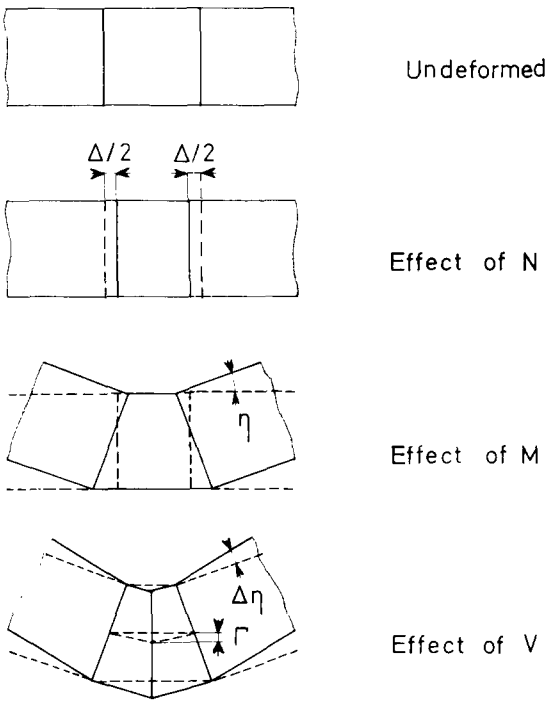

FIG. 8. The successive deformations of a hinge when subjected to various forces.

inception of the plastic collapse will be similar to that shown in Fig. 9. Note that shear deformation at hinge A implies a small rotation $\Delta\eta$ at A and B, in turn causing a small rotation ξ at the support. It should also be noted that at hinge B a shear deformation does not exist, since at this location v_B was set equal to zero.

It could be easily verified that the horizontal and vertical motions of the central hinge are given by

$$\mathbf{u} = -(\psi-\eta+\xi)(1-\cos\phi_0)R+(\psi+\Delta\eta+\xi)[1-\cos(\phi_0-\chi)]R + \Delta_B\cos(\phi_0-\chi)+\tfrac{1}{2}\Delta_A = 0 \tag{16a}$$

$$\mathbf{v} = -(\psi-\eta+\xi)R\sin\phi_0+(\psi+\Delta\eta+\xi)R\sin(\phi_0-\chi) - \Delta_B\sin(\phi_0-\chi)+\tfrac{1}{2}\Gamma_A. \tag{16b}$$

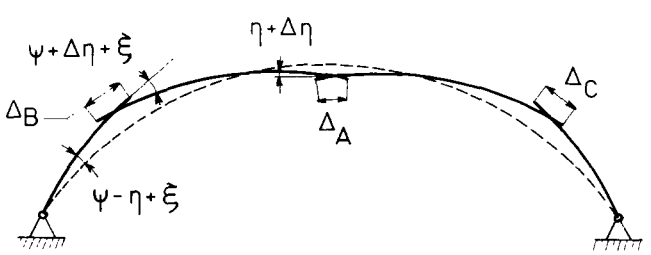

FIG. 9. Failure mechanism of the arch.

However, since the velocities at hinges are not independent, one must seek the proper relationship among them. Now, let the total rotation rates be denoted:

$$\psi+\Delta\eta+\xi = -\theta_B \quad \text{and} \quad \eta+\Delta\eta = \theta_A/2. \tag{17}$$

Consequently:

$$\psi-\eta+\xi = -\theta_B-\theta_A/2. \tag{18}$$

The sign of any strain-rate component may be verified with reference to the location of the stress point on the yield surface, i.e. equations (12) and Fig. 10.

Similarly, for the shortening rates, one has

$$\begin{aligned} \Delta_A &= \frac{M_0}{N_0}\lambda_A \\ \Delta_B &= \frac{M_0}{N_0}\lambda_B \end{aligned} \tag{19}$$

where λ_A and λ_B are non-dimensional shortening rates, both having negative signs.

Finally, the shearing rates are:

$$\begin{aligned} \Gamma_A &= \frac{M_0}{V_0}\gamma_A \\ \Gamma_B &= 0 \end{aligned} \tag{20}$$

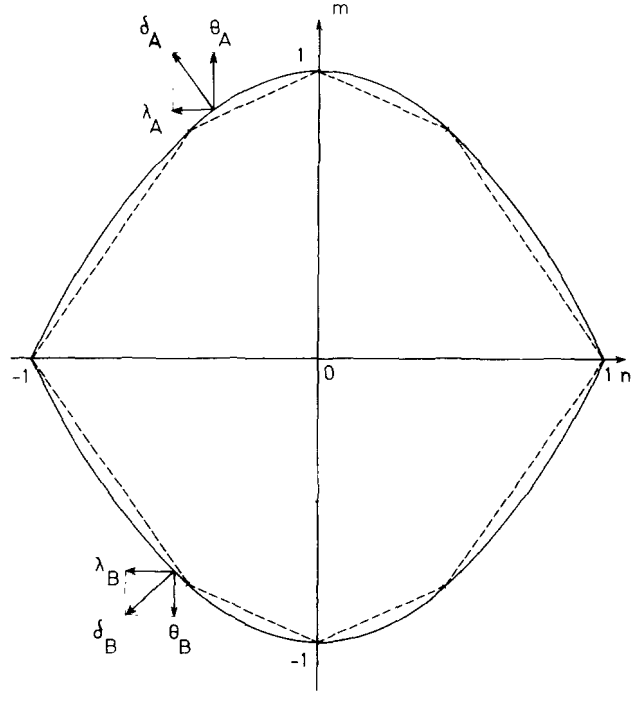

FIG. 10. The yield interaction in the absence of shear force.

where γ_A is the non-dimensional shearing rate at the central hinge. Because of the symmetry, the horizontal velocity, equation (16a), at the hinge A is equal to zero, from which one gets:

$$\frac{\theta_A}{2\theta_B} = \frac{\cos\phi_0 - \left(1 + \dfrac{M_0}{N_0 R}\dfrac{\lambda_B}{\theta_B}\right)\cos(\phi_0 - \chi)}{1 - \cos\phi_0 + \dfrac{M_0}{N_0 R}\dfrac{\lambda_B}{\theta_B}}. \tag{21}$$

Substitution of relation (21) in the expression of the vertical motion of the central hinge, equation (16b), results in:

$$\frac{\mathbf{v}}{R\theta_B} = \sin\phi_0 - \left(1 + \frac{M_0}{N_0 R}\frac{\lambda_B}{\theta_B}\right)\sin(\phi_0 - \chi) + \frac{\theta_A}{2\theta_B}\left(\sin\phi_0 + \frac{M_0}{V_0 R}\frac{\gamma_A}{\theta_A}\right). \tag{22}$$

The rate of the external work done by the applied load $2P$, may then be expressed as:

$$\begin{aligned} W_{\text{ext}} &= 2P\mathbf{v} \\ &= 2PR\theta_B\left[\sin\phi_0 - \left(1 + \frac{M_0}{N_0 R}\frac{\lambda_B}{\theta_B}\right)\sin(\phi_0 - \chi) + \frac{\theta_A}{2\theta_B}\left(\sin\phi_0 + \frac{M_0}{V_0 R}\frac{\gamma_A}{\theta_A}\right)\right]. \end{aligned} \tag{23}$$

The rate of the internal work is given by:

$$\begin{aligned} W_{\text{int}} &= M_0[(m_A\theta_A + v_A\gamma_A + n_A\lambda_A) + 2(m_B\theta_B + n_B\lambda_B)] \\ &= 2M_0\theta_B\left[\frac{\theta_A}{2\theta_B}\left(m_A + v_A\frac{\gamma_A}{\theta_A} + n_A\frac{\lambda_A}{\theta_A}\right) + \left(m_B + n_B\frac{\lambda_B}{\theta_B}\right)\right]. \end{aligned} \tag{24}$$

Since no energy can be stored in the rigid-plastic arch, the rate of energy dissipation must be equal to the rate of work done by the external load, i.e.

$$W_{\text{int}} = W_{\text{ext}}$$

from which:

$$\rho^+ = \frac{\dfrac{\theta_A}{2\theta_B}\left(m_A + v_A\dfrac{\gamma_A}{\theta_A} + n_A\dfrac{\lambda_A}{\theta_A}\right) + \left(m_B + n_B\dfrac{\lambda_B}{\theta_B}\right)}{\sin\phi_0 - \left(1 + \dfrac{M_0}{N_0 R}\dfrac{\lambda_B}{\theta_B}\right)\sin(\phi_0 - \chi) + \dfrac{\theta_A}{2\theta_B}\left(\sin\phi_0 + \dfrac{M_0}{V_0 R}\dfrac{\gamma_A}{\theta_A}\right)} \tag{25}$$

where $\rho^+ = PR/M_0$.

Expressions (14) and (25) give lower and upper bound on the collapse load of the arch.

3.3 *Numerical results*

Equations (15) were programmed on a digital computer, and the variable χ, found from the solution of these equations, was substituted in (12) and (14). Thus, the stress values m_A, m_B, n_A, n_B, v_A and the lower bound to the collapse load ρ^- were calculated. For the upper bound analysis, the strain-rate ratios λ_A/θ_A, γ_A/θ_A and λ_B/θ_B have to be computed. For the hinge B, consideration of the normality to the yield surface (13) (Fig. 10) yields

$$\frac{\lambda_B}{\theta_B} = -2n_B. \tag{26}$$

For the central hinge, let the total strain-rate vector be denoted by δ_A. The direction cosines may then be specified as θ_A/δ_A, γ_A/δ_A and λ_A/δ_A, respectively (Fig. 3). The parametric equations of the interaction surface are given by relations (9), therefore, the direction cosines will have the values:

$$\frac{\theta_A}{\delta_A} = \frac{K_1}{K} \qquad \frac{\gamma_A}{\delta_A} = \frac{K_2}{K} \qquad \frac{\lambda_A}{\delta_A} = \frac{K_3}{K} \tag{27}$$

where

$$K_1 = v'_r n'_s - v'_s n'_r \qquad K_2 = m'_r v'_s - m'_s v'_r$$
$$K_3 = n'_r m'_s - n'_s m'_r \qquad K = (K_1^2 + K_2^2 + K_3^2)^{\frac{1}{2}}$$

and a prime over the dimensionless generalized stresses m, n and v denotes partial differentiation with respect to the variable shown as a subscript, i.e.

$$n'_s = \frac{\partial n(r, s)}{\partial s}, \quad v'_r = \frac{\partial v(r, s)}{\partial r}, \text{ etc.} \tag{28}$$

The strain-rate ratios evaluated from (27), are then substituted in equation (25) which yields an upper bound to the collapse load.

The upper and lower bounds computed for a wide range of parameters involved, give identical values. The solution presented here, is therefore, an exact one, although equations (12) and (25) cannot be analytically deduced identical. This is due to the transcendental and parametric nature of the equations involved. However, as will be shown in the next section, for a particular case of the problem treated here, an analytical deduction becomes possible.

Figure 11 shows the collapse load as a function of angle ϕ_0 for various values of thickness to diameter ratio, $t = h/R$. It is evident that the limit load is very sensitive to t. On the other hand, if one plots the collapse load against t for various values of ϕ_0, one will note that the effect of ϕ_0 is pronounced only at small angles and/or small values of t.

3.4 *Special case—no shear effect*

The collapse load of a two-hinged circular arch of uniform rectangular cross-section, carrying a single vertical load at the center of its span, was first obtained by Onat and Prager [6]. However, the analysis was based on the piece-wise linearized curve of Fig. 10, in addition to neglecting the effect of shear force in yielding of the arch. Hodge [8] later extended the analysis to cover other ranges of geometric parameters. Here, the same problem will be treated as a special case of the solution given earlier. However, the exact (non-linear) interaction curve will be considered. In this sense, even the results presented here as a special case are an improvement over the works of Refs. [6, 8].

In the lower bound approach, it is only sufficient to determine angle χ and replace it in the relation (14). The stress point at the central hinge A, when shear effect on yielding is omitted, will be on the curve shown on Fig. 10:

$$m_A = 1 - n_A^2. \tag{29}$$

From relations (13) and (29) one then gets the identity:

$$\cos\chi - \cos(\phi_0 - \chi) - (1 - \cos\chi) = \frac{CA^2}{4}\rho \sin(\phi_0 - \chi). \tag{30}$$

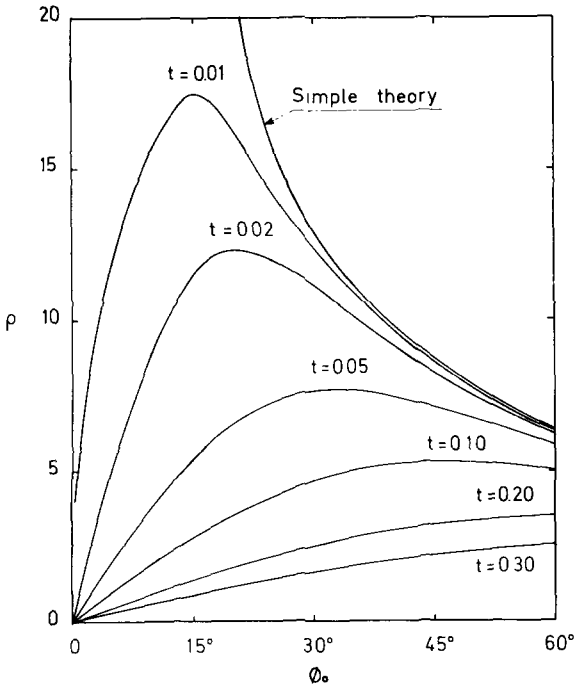

FIG. 11. The variation of collapse load vs. arch semi-angle ϕ_0 for various values of thickness to diameter ratios.

The value of ρ substituted from (14) results in the following relation:

$$\cos\chi-\cos(\phi_0-\chi)-(1-\cos\chi)$$
$$-\tfrac{1}{2}\sin^2(\phi_0-\chi)\{[(1-\cos\chi)^2+CA^2]^{\frac{1}{2}}-(1-\cos\chi)\}=0 \tag{31}$$

from which χ can be determined.

For the upper bound, it suffices to set $\gamma_A = 0$ in equation (25), which gives:

$$\rho^{*+}=\frac{\dfrac{\theta_A}{2\theta_B}\left(m_A+n_A\dfrac{\lambda_A}{\theta_A}\right)+\left(m_B+n_B\dfrac{\lambda_B}{\theta_B}\right)}{\sin\phi_0-\left(1+\dfrac{M_0}{N_0R}\dfrac{\lambda_B}{\theta_B}\right)\sin(\phi_0-\chi)+\dfrac{\theta_A}{2\theta_B}\sin\phi_0} \tag{32}$$

where $\theta_A/2\theta_B$ is given by equation (21), χ by equation (31) and noting that from (24),

$$\frac{\lambda_A}{\theta_A}=-\frac{\mathrm{d}m_A}{\mathrm{d}n_A}=2n_A. \tag{33}$$

Replacing all the terms in (32) by their appropriate expressions in function of ρ^{*-} and χ, one gets, after performing some algebraic manipulations,

$$\rho^{*+}=\rho^{*-}. \tag{34}$$

Thus the solution given here is an exact one.

Figure 12 shows the comparison between the limit pressures predicted here and that of Hodge [8]. As stated earlier, the solution in Ref. [8] is based on a piecewise linearized interaction curve, Fig. 10. If the exact parabolic curve is denoted by f_T, and the linearized approximation by f_{lin}, the relation between the two interaction diagrams then will be:

$$f_{\text{lin}} < f_T \leq 1{\cdot}062 f_{\text{lin}}. \tag{35}$$

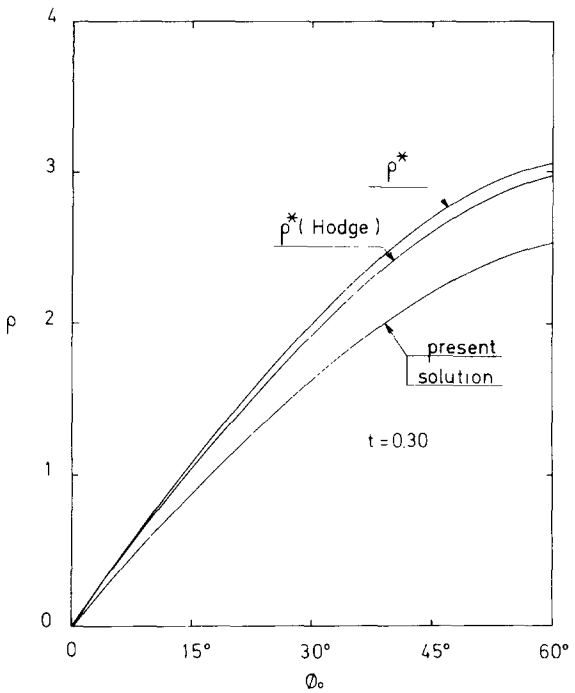

FIG. 12. The comparison of limit loads as predicted by various theories.

The bounding surface lemma states that the same relation must exist among the predicted collapse loads. The comparison between the special case solution given here and that of Ref. [8] shows that the limit loads of the arch are indeed bounded by relation (35). On Fig. 12, in addition, the limit pressure obtained by considering the shear effect in yielding i.e. equations (14) or (25), is plotted. The difference between the latter predictions and that of no shear effect increases as t is increased. Figure 13 shows the variation, in percentage, of the extreme deviation with respect to t for arch semi-angles up to 60°. The results seem to indicate that for arches with thickness to diameter ratio $t < 0{\cdot}1$, the effect of shear force on the yielding may be neglected. For thicker arches, omission of the shear effect will result in over-estimation of the load carrying capacity.

The limit load predicted by "simple" theory (moment effect only) is considerably higher and falls outside the scale of Fig. 12. It is however, included in Fig. 11 for the sake of comparison.

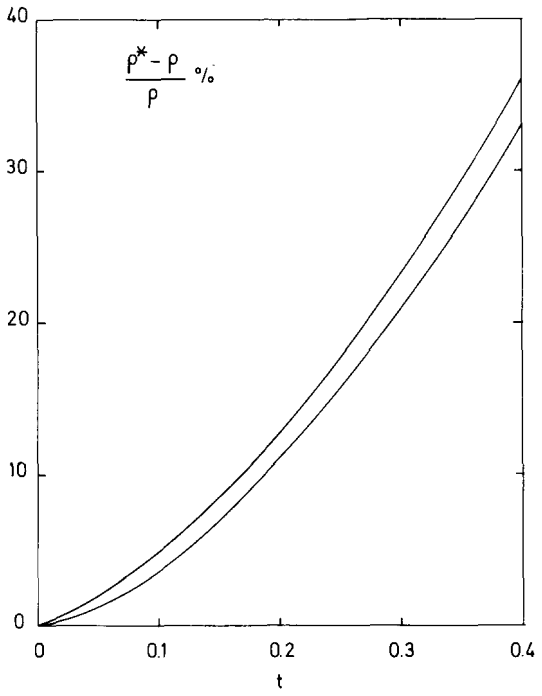

FIG. 13. Bounds of shear effect on collapse load of arches with ϕ_0 up to 60°.

4. CONCLUSIONS

Exact interaction surfaces for structural elements subject to combined axial force, shear force and bending moment, are obtained. The analysis is based on the consideration of moment, axial and shear force, as generalized stress variables. The intersection of the interaction diagram with planes v = const. shows that up to a certain value of plastic shear force, the influence of V on M–N curve is negligible.

A simply supported arch is considered for the application of the theory. Complete solutions are obtained when either including or excluding the shear effect in yielding. The results presented show that for $t \leq 0{\cdot}1$, the shear influence may be neglected. However, for $t \geq 0{\cdot}1$ the simple theory will over-estimate the load carrying capacity of arches, and the effect of shear should be taken into consideration. The change in geometry of the arch is not taken into account in the present analysis. The influence of geometric change will not be noticeable in the range of parameters where shear effect is pronounced. The approach proposed here may be extended to plate problems.

Acknowledgements—The work reported here forms part of a general investigation on elastic–plastic behaviour of structures. The research is sponsored by the National Research Council of Canada (Grant A-3803) and Ministère de l'Education du Gouvernement du Québec.

REFERENCES

[1] D. C. DRUCKER, The effect of shear on the plastic bending of beams. *J. appl. Mech.* **23**, 509–514 (1956).
[2] W. PRAGER, The General Theory of Limit Design, *Proceedings of the Eighth International Congress of Theoretical and Applied Mechanics*, Istanbul, Turkey, 1952, vol. 2, pp. 65–72 (1956).

[3] P. G. HODGE, JR., Interaction curves for shear and bending of plastic beams. *J. appl. Mech.* **24**, 453–456 (1957).
[4] D. C. DRUCKER, A more Fundamental Approach to Plastic Stress–Strain Relations, *Proceedings of the First U.S. National Congress of Applied Mechanics*, Chicago, 1951, pp. 487–491. J. W. Edwards (1952).
[5] J. HEYMAN, The full plastic moment of an *I*-beam in the presence of shear force. *J. Mech. Phys. Solids* **18**, 359–365 (1970).
[6] E. T. ONAT and W. PRAGER, Limit analysis of arches. *J. Mech. Phys. Solids* **1**, 77–89 (1953).
[7] C. E. MASSONNET and M. A. SAVE, Necessary Conditions for the Existence of the Plastic Moment. Variables Influencing its Value, *Plastic Analysis and Design*, Chapter 5, pp. 128–135. Blaisdell (1965).
[8] P. G. HODGE, JR., Axial Forces in Frames and Arches, *Plastic Analysis of Structures*, Chapter 7, pp. 182–191. McGraw-Hill (1959).

(*Received* 19 *April* 1971; *revised* 30 *August* 1971)

Абстракт—Получаются поверхности взаимодействия для элементов конструкций, подверженных совместному действию осевого сдвигающего усилий и изгибного момента. Подразумевается, что конструкционный материал жестко-идеально-пластический, удовлетворящий условию текучести Трески или Мизеса. Дается пример двухшарнирной круглой арки, с целью представления применения предлагаемой теории. Эффект учета силы сдвига уменьшает нагрузку разрушения. Указываются пределы, для которых влияние силы сдвига на течение арок является значительным.